

An Inverse, Decision-Based Design Method for Robust Concept Exploration

Anand Balu Nellippallil¹

School of Aerospace and Mechanical Engineering,
University of Oklahoma,
Norman, OK 73019
e-mails: anand.balu@ou.edu;
anand.nellippallil@msstate.edu

Pranav Mohan²

School of Aerospace and Mechanical Engineering,
University of Oklahoma,
Norman, OK 73019
e-mail: pm@ou.edu

Janet K. Allen³

School of Industrial and Systems Engineering,
University of Oklahoma,
Norman, OK 73019
e-mail: janet.allen@ou.edu

Farrokh Mistree

School of Aerospace and Mechanical Engineering,
University of Oklahoma,
Norman, OK 73019
e-mail: farrokh.mistree@ou.edu

In this paper, we extend our previous work on a goal-oriented inverse design method to carry out inverse robust design by managing the uncertainty involved. The extension embodies the introduction of specific robust design goals and new robust solution constraints anchored in the mathematical constructs of Error Margin Indices (EMIs) and Design Capability Indices (DCIs) to determine “satisficing” robust design specifications across analytical model-based process chains. Contributions in this paper include the designer’s ability to explore satisficing robust solution regions when multiple conflicting goals and multiple sources of uncertainty are present. Using the goal-oriented inverse design method, robust solutions are propagated in an inverse manner. We demonstrate the efficacy of the method and the associated robust design functionalities using an industry-inspired hot rolling and cooling process chain example problem for the production of a steel rod. In this example, we showcase the formulation of multiple mechanical property goals for the end product using the robustness metrics and the exploration of satisficing robust solutions for material microstructure after the cooling process using the robust solution constraints. The robust solutions thus identified are communicated in an inverse manner using the design method to explore satisficing robust solutions for the microstructure generated after the hot rolling process. Using the example, we demonstrate the robust co-design of material, product, and associated manufacturing processes. The method and the associated design constructs are generic and support the formulation and inverse robust design exploration under uncertainty of similar problems involving a sequential, analytical model-based flow of information across process chains.

[DOI: 10.1115/1.4045877]

Keywords: robust design, uncertainty management, materials, products, manufacturing process design, inverse decision-based design method, computer-aided design, simulation-based design, systems design

1 Frame of Reference

In practice, design involved the selection of a suitable material for a given application [1–4]. The discovery of new materials has always been arduous, fortuitous, and instinctive for the people in this domain. A materials design revolution is underway in the recent past. The focus here is to design the material microstructure and processing paths to achieve multiple property or performance requirements that are often in conflict in a “top-down” (goal-oriented) manner as advocated by Olson [5]. To realize the same at the early stages of design, we seek top-down (goal-oriented or inverse) methods to carry out design exploration of the processing paths and material microstructures that meets a set of specified property/performance requirements. The words “goal-oriented” and “inverse” here are used to denote our approach of top-down systems design where the focus is to design the system and sub-systems starting from some end performance goals in an inverse manner. Many have highlighted the challenges associated with the top-down (goal-oriented/inverse) approach of materials design, see Refs. [6–9]. Among these are the challenges arising due to (i) uncertain material models (that includes input factors, parameters, responses, etc.) due to simplification/idealization or a lack of

complete knowledge, (ii) the propagation of uncertainty from different sources as information flows from one to model to another, and (iii) the lack of domain-independent design “exploration” methods and tools for the early stages of design. An effective inverse approach for materials design must address the uncertainty of models and experiments at each scale, as well as uncertainty propagation through a chain of models and/or experiments at different levels of hierarchy with the ability to provide decision support through rapid design space exploration [8]. We address each of these challenges next.

The sources of uncertainty could be the following [6]: the natural uncertainty inherent in a system, the uncertainty associated with model parameters, the uncertainty inherent in models, and the propagation of all these information flows from one model to another. Two approaches are typically followed in dealing with these sources of uncertainty—(i) mitigating uncertainty and (ii) managing uncertainty. In the first approach, the focus is to reduce/mitigate the uncertainty by seeking “perfect” models, collecting more data and developing improved methods to model, calculate, and quantify uncertainty through expensive computations. There are several recent works in this vein using Bayesian networks (see Refs. [10–13]) and modern data science methods and microstructure informatics (see [14–17]). However, McDowell [8] observes that quantifying uncertainty in schemes for linking models at different lengths and timescales is still an immature field, and formal mathematical approaches for doing this are largely undeveloped. This demands the need for the second approach of managing uncertainty by designing the system to be insensitive to the sources without reducing or eliminating them. This is done by exploring the solution space and studying the sensitivity of responses to variations in noise, control factors, and models and understanding the trade-offs

¹Currently at: Center for Advanced Vehicular Systems, Mississippi State University, Starkville, MS 39759.

²Currently at: School of Mechanical Engineering, Purdue University, West Lafayette, IN 47907-2088.

³Corresponding author.

Contributed by the Design Automation Committee of ASME for publication in the JOURNAL OF MECHANICAL DESIGN. Manuscript received September 26, 2018; final manuscript received October 23, 2019; published online January 6, 2020. Assoc. Editor: Mian Li.

required with various compromises, defined as a robust design and classified into mainly three categories [6]: (i) Type I robust design where designers seek to design insensitive to variation due to noise factors, (ii) Type II robust design where designers seek to design insensitive to variation due to control factors, (iii) Type III robust design where designers seek to design insensitive to variation due to uncertainty inherent in models.

In Fig. 1, different sources of uncertainty (dashed ellipses) and corresponding robust designs in the model-based realization of complex systems are shown. The focus on the robust design is not on extensive optimization searches at individual levels and do not necessarily involve a large number of iterations [18]. The practical interest here is for a ranged set of satisficing solutions that showcase good performance under variability rather than single-point solutions that are valid for a narrow range of conditions while performing poorly when the conditions are changed slightly. The term satisficing used in this context is coined by Simon [19] and is foundational to our approach to decision-based design. As part of the “satisficing” community, our intention in this paper from the design side is to satisfy (satisfy and suffice) a set of conflicting goals and explore robust solutions, defined as “satisficing robust solutions,” in an inverse manner by managing uncertainty.

Given the requirement of managing uncertainty, we next address the issue of inverse design exploration using domain-independent design methods and tools. Materials design using inverse methods is gaining a lot of attention in the recent past. There are several recent efforts toward this. Adams et al. [20] propose a framework and utilize highly efficient spectral representations to arrive at invertible linkages between material structure, its properties, and their corresponding processing paths. Kalidindi et al. [21,22] propose the Material Knowledge Systems approach and showcase the advances in rapid inverse design to estimate local responses. These inverse design approaches, however, demand considerable knowledge and insight into mechanisms, material hierarchy, and information flow and are mostly suited for detailed design and not for “design exploration” [8]. We recognize that approaches to pursue inverse design exploration using system-based design especially at early stages of design are limited and need further evaluations to address hierarchical material design problems with the consideration of robustness. Choi et al. [23] propose the compromise Decision Support Problem formulation with Error Margin Index (EMI) for Types I, II, and III robust design. However, their work is limited as they address only: (i) a single-objective case and not when multiple design objectives/goals are present, (ii) a single robust design formulation using EMI when all sources of uncertainty classified exists in a problem formulation, which is typically not the case when multiple goals exist. The inductive design exploration method (IDEM) proposed by Choi et al. [24] is another multi-level, top-down, robust design exploration method that considers the propagation of model parameter and model structure uncertainty across process chains. However, there are certain limitations to IDEM. These include limitations in terms of (i) errors due to discretization of design space resulting in the inability to capture the feasible

boundary accurately that leads to loss of information, (ii) highly computationally expensive IDEM runs if the accuracy is increased, (iii) the number of design variables (impossible beyond nine variables) that can be studied thereby limiting the problem size, (iv) exploration and visualization as IDEM involves a three-dimensional visualization space using HD-EMI metric for exploration where only a maximum of three design variables can be studied at a time with the others variables taking defined values, and (v) flexibility in the design as IDEM does not allow designers to incorporate new goals or requirements at different levels during the design process as the method is based on mapping to feasible spaces. Nellippallil et al. [25] propose an inverse, decision-based design method known as goal-oriented inverse design (GoID) addressing some of these limitations. The GoID method offers (i) an increase in problem size as there are no limitations in the number of design variables and goals to be studied, (ii) improved flexibility in the design of the various processes involved as individual design spaces are formulated at each level allowing designers to incorporate new design goals and requirements, and (iii) the capability to visualize and explore “satisficing” solutions for multiple conflicting goals. However, the idea of robustness under uncertainty is not captured in the GoID in its current form as defined in Ref. [25] and is, therefore, a limitation.

In this paper, we extend the existing goal-oriented inverse design method proposed by Nellippallil et al. [25] to bring in robustness for multiple goals from the standpoint of Types I to III robust design across process chains. The extension embodies the introduction of specific robust design goals, constraints, and metrics to determine “satisficing robust design” specifications for given performance requirement ranges using the goal-oriented, inverse design method. The primary mathematical construct used in the extended inverse method is the compromise Decision Support Problem with Error Margin Index [23] and Design Capability Index [26] (compromise Design Support Problem (cDSP) with EMI–DCI) supported by the Concept Exploration Framework (CEF) to generate satisficing Types I, II, and III robust design solutions across process chains. We hypothesize that the EMIs and DCIs, when used together in search algorithms, are capable of helping the designer in designing the system robust to both model parameter and model structure uncertainty. Contributions in this paper include the designer’s ability to explore “satisficing robust solution” regions when multiple conflicting goals and multiple sources of uncertainty are present. The extended method and robust design constructs are suitable for problems in which clearly defined analytical models/functions are either available or can be developed to capture the problem-specific information. In this paper, an industry-inspired example problem, namely the design of a hot rolling and cooling process chain for the production of a steel rod is used as an example to demonstrate the efficacy of the method and the associated robust design constructs for the inverse robust design under uncertainty of the material, product, and manufacturing processes. In Sec. 2, we describe the CEF and the cDSP-EMI–DCI construct for the robust concept exploration.

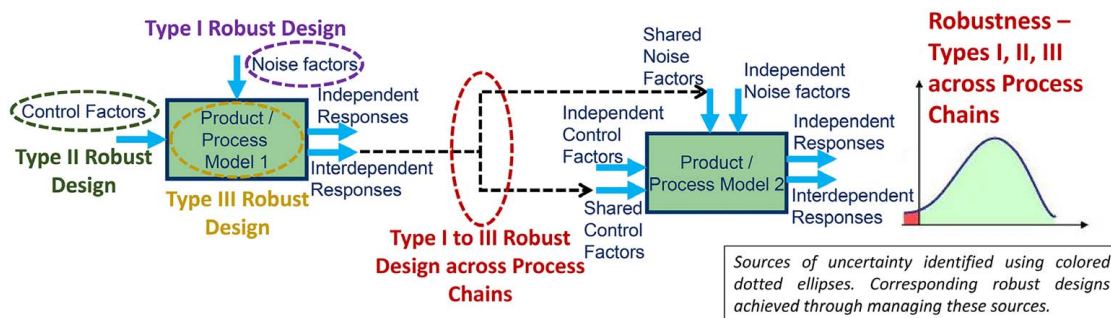


Fig. 1 The sources of uncertainty and corresponding robust designs in complex material, product, and process systems

2 The Concept Exploration Framework For Types I, II, and III Robust Design

The Concept Exploration Framework is a mathematical framework that includes systematic steps to generate design alternatives by exploring the solution space and identify satisficing design specifications.

We recognize that a framework that supports robust concept exploration in integrated material, product, and process design should satisfy three requirements: (i) computational efficiency, (ii) generic enough to be applicable to various levels of material design hierarchy, and (iii) incorporation of Type I, II, and III robust design formulations for multiple conflicting goals. In this paper, we update the CEF to include the compromise Decision Support Problem with Error Margin Index and Design Capability Index together in a single formulation to take into account complex material and product design problems that require combinations of Type I, II, and III robust designs. In Fig. 2, we show the modified CEF with the incorporation of robust design goals and constraints in the cDSP using the EMIs and DCIs. The systematic steps associated with the CEF to generate satisficing design specifications remains the same as defined in Ref. [25] and are not repeated here. The eight processors (A, B1, B2, D, E, F, G, and H) and simulation programs (C) defined in the CEF support systematic problem formulation, systematic solution space exploration and thereby

provide decision support for any complex systems problem. In this paper, we address robust concept exploration for instantiating Type I, II, and III robust designs and therefore focus on processors A, F, and H of the CEF shown in Fig. 2. The formulation of a cDSP with EMI and DCI using the CEF involve (a) quantification of variability and model parameter uncertainty, (b) formulation of error margin indices and design capability indices and incorporating them in the cDSP, and (c) robust decision-making by exploration of solution space by executing the cDSP with EMI–DCI. Choi et al. [23] explain in detail on quantifying variability and model parameter uncertainty. They use response modeling approach for quantifying response variability due to parameterizable noise factors and location and dispersion modeling approach for quantifying unparameterizable variability. However, we observe that for problems related to complex manufacturing processes involving materials and products like hot rolling and cooling, several studies are already carried out and different models defining material/process behavior are available in the literature [27–33]. These models are either based on natural laws or based on experiments/modeling. Such available theoretical and empirical models when directly used to formulate the cDSP do not require the response modeling-based approach followed by Choi and coauthors as the variability can be assessed directly using the functional relations. In the approach proposed using the CEF, one major assumption is that models (mean models and their variabilities) in the form of

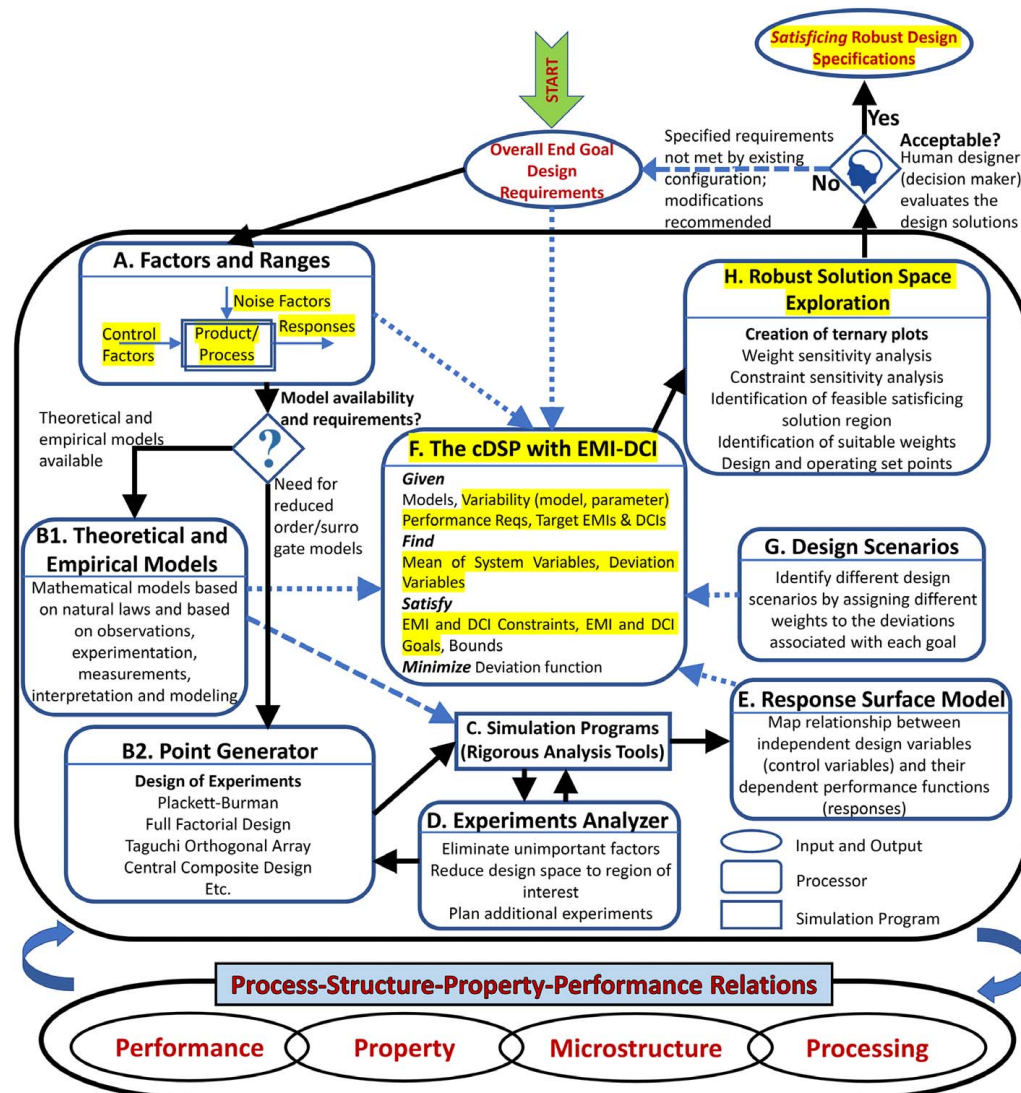


Fig. 2 The modified Concept Exploration Framework for Types I, II, and III robust design

analytical functions are either available or can be developed by carefully planned design experiments. One major limitation therefore of the proposed approach is its inapplicability when models in the form of analytical equations are not available. Next, we discuss the formulation of EMI and DCI using functional relations and information available.

2.1 Formulation of Design Capability Indices and Error Margin Indices. Design Capability Indices and Error Margin Indices are metrics for system performance and robustness. Design Capability Indices represent the amount of safety margin against system failure due to uncertainty in the system variables while EMIs represent the margin against failure due to uncertainty in both model and design variables. Both are dimensionless. The EMIs support Types I, II, and III robust designs while DCIs support Type I and II robust designs. We briefly describe the steps involved in formulating and calculating DCIs and EMIs for two types of systems, respectively.

2.1.1 Design Capability Indices for Systems Having Variability in Design Variables Only. *Step 1:* Using the first-order Taylor series expansion, estimate the response variation due to variation in the design variable vector $x = \{x_1, x_2, \dots, x_n\}$. The response variation (ΔY) for small variations in design variables is

$$\Delta Y = \sum_{i=1}^n \left. \frac{\partial f}{\partial x_i} \right| \Delta x_i \quad (1)$$

Step 2: Using the mean response (μ_y) obtained from the mean response model ($f_0(x)$) and the response variation due to variation in design variables (ΔY), calculate the DCIs. For a “Larger is Better” case, the DCI is calculated as

$$\text{DCI} = \frac{\mu_y - \text{LRL}}{\Delta Y} \quad (2)$$

where *LRL* is the lower requirement limit. A $\text{DCI} \geq 1$ means that the ranged set of design specifications satisfies a ranged set of design requirements and the system is robust against model parameter uncertainty. Higher the value of DCI, higher is the measure of safety against failure due to model parameter uncertainty.

2.1.2 Error Margin Indices for Systems Having Variability in Both Models and Design Variables. *Step 1:* Assuming a system model has k uncertainty bounds, calculate the response variation (ΔY_j) for each of them for a small variation in design variables as

$$\Delta Y_j = \sum_{i=1}^n \left. \frac{\partial f_j}{\partial x_i} \right| \Delta x_i \quad (3)$$

where $j=0, 1, 2, \dots, k$ (number of uncertainty bounds).

In Fig. 3(a), we show a mean response model (solid curve) with two uncertainty bounds (the dotted curves). In the left side of Fig. 3(a), we show the response variations of mean function and uncertainty bound functions with respect to the variations in design variables.

Step 2: After evaluating the multiple response variations of mean response function and the k uncertainty bound functions for variations in design variables, calculate the minimum and maximum responses by considering the variability in design variables and uncertainty bounds around the mean response as

$$Y_{\max} = \text{Max}[f_j(x) + \Delta Y_j] \text{ and} \quad (4)$$

$$Y_{\min} = \text{Min}[f_j(x) - \Delta Y_j] \quad (5)$$

where $j=0, 1, 2, \dots, k$ (number of uncertainty bounds), $f_0(x)$ is the mean response function, and $f_1(x) \dots f_k(x)$ are the uncertainty bound functions

Step 3: Calculate the upper and lower deviations of response at x as

$$\Delta Y_{\text{upper}} = Y_{\max} - f_0(x) \text{ and} \quad (6)$$

$$\Delta Y_{\text{lower}} = f_0(x) - Y_{\min} \quad (7)$$

Step 4: Using the mean response (μ_y) obtained from the mean response model ($f_0(x)$) and the upper and lower deviations (ΔY_{upper} and ΔY_{lower}), calculate the EMIs. For a “Larger is Better” case, the EMI is calculated as

$$\text{EMI} = \frac{\mu_y - \text{LRL}}{\Delta Y_{\text{lower}}} \quad (8)$$

The EMI thus calculated for “Larger is Better” case will be larger when the location of μ_y is farther away from the LRL and/or when ΔY_{lower} gets smaller, as shown in Fig. 4. An $\text{EMI} = 1$ means that the uncertainty bound just meets the requirements limit. An $\text{EMI} \leq 1$ means that the requirement limit may get violated due to the uncertainty in the model and design variables. The same can be derived from other cases shown in Fig. 3(b) for both EMI and DCI.

2.2 The compromise Design Support Problem With Error Margin Indices—Design Compatibility Indices for Robust Design Types I, II, and III. Core to the CEF is the foundational mathematical construct—the compromise Decision Support Problem (cDSP). The cDSP construct is anchored in the robust design paradigm first proposed by Taguchi and Clausing [34]. The fundamental assumption here is that the models are not complete, accurate, and of equal fidelity [35]. The cDSP is a hybrid of mathematical programming and goal programming. Target values for each of the goals are defined in the cDSP, and the emphasis of the designer is to satisfy these target goals as closely as possible. This is achieved by seeking multiple solutions through trade-offs among multiple conflicting goals. The solutions obtained are further evaluated by solution space exploration to identify solution regions that best satisfy the requirements identified. There are four keywords in the cDSP—Given, Find, Satisfy, and Minimize. The overall goal of the designer using the cDSP is to minimize a deviation function—a function formulated using the deviations (captured using deviation variables) that exists from the goal targets. The details regarding formulating and solving the cDSP are available [35] and are not explained here. The mathematical formulation of the cDSP with EMI and DCI goals and constraints to achieve robust design Types I, II and III is shown in Table 1.

In the cDSP formulation, mean response functions for different multiple performance goals $f_{0,i}(x)$, the upper and lower uncertainty bound functions for those goals with model uncertainty, $f_{1,i}(x)$ and $f_{2,i}(x)$ are captured. System constraints and goals in terms of EMI and DCI are formulated in the cDSP to capture the designer’s requirements and the functionalities desired in the material-product system. The lower requirement limits (LRLs) and upper requirement limits (URLs) are defined for the system. The uncertain system constraints are captured as EMI constraints, $s_i(x)$ or $\text{DCI}_{\text{constraints},i}(x) \geq 1$ using $g_i(x)$ functions depending on the type of variability. We propose new constraints, defined as *robust solution constraints* in our cDSP formulation to ensure the identification of robust solutions always when preferences are changed for the different goals. These constraints ensure both EMI and DCI are greater than or equal to 1 for all design scenarios during solution space exploration (in order to identify robust solutions). In this paper, we address multiple conflicting goals and there could be situations where when achieving EMI and/or DCI greater than 1 for one goal could result in EMI and/or DCI less than 1 for the other goal. To prevent this, we introduce the EMI, DCI constraints for the goal functions. This approach will result in a solution space of only robust solutions to be explored we define it as “robust solution space exploration” for multiple conflicting goals. From these robust solutions, the designer chooses the range of solutions that best satisfies his/her interest. We define this

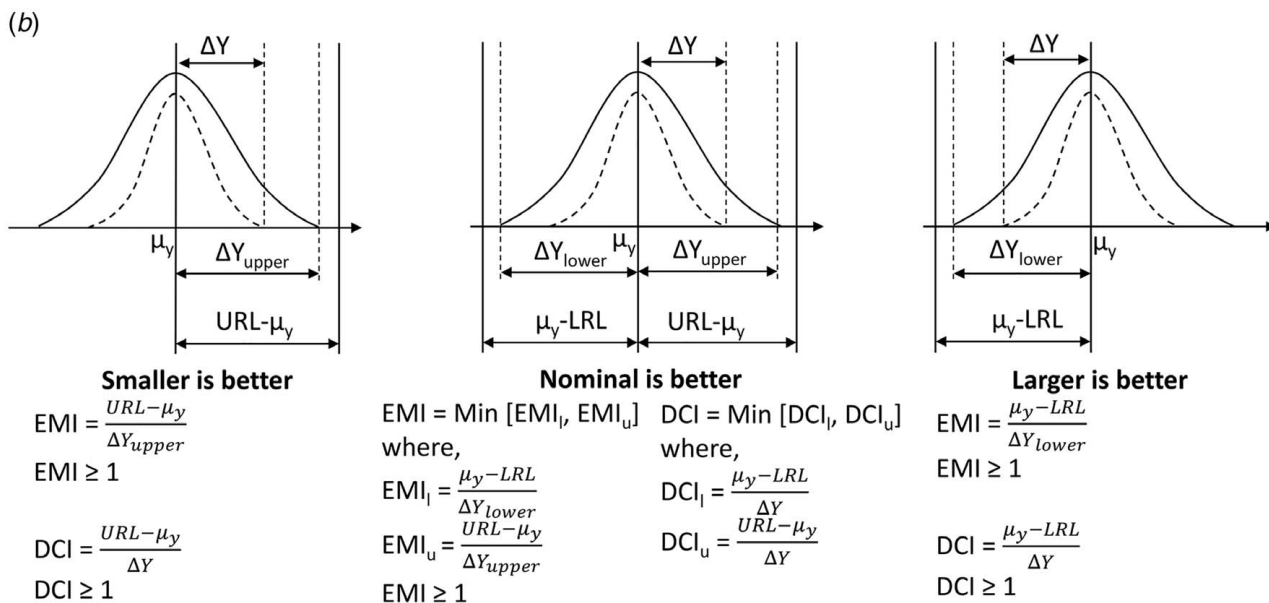
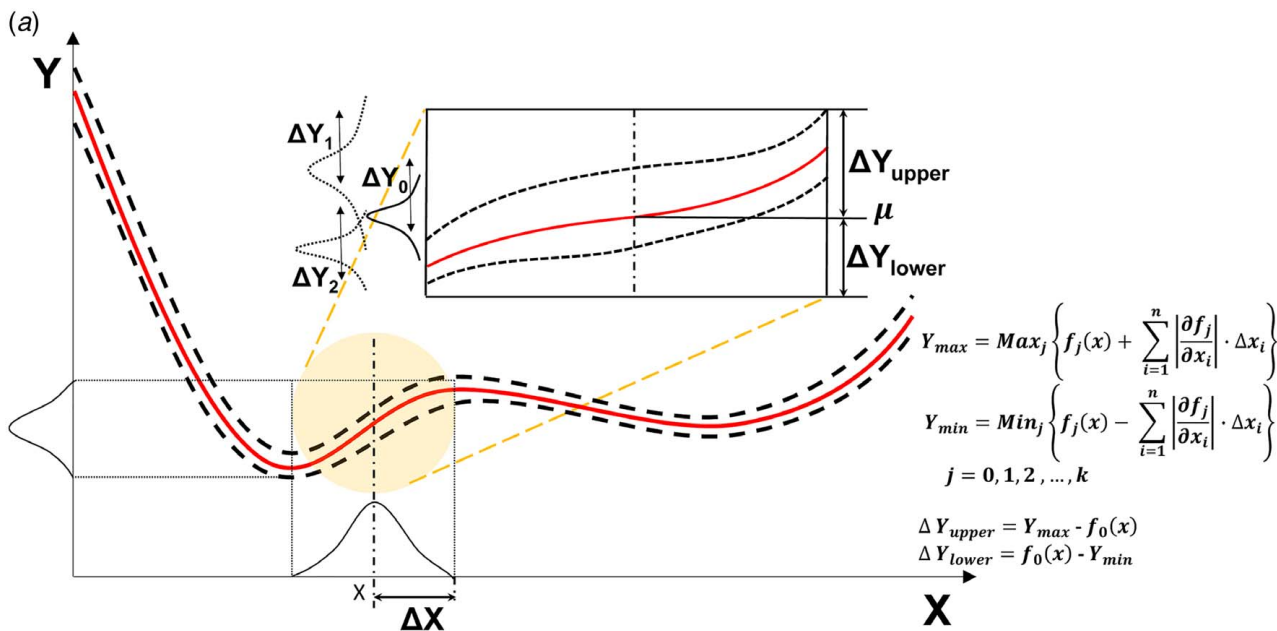


Fig. 3 (a) Uncertainty bound formulation for variability in design variable and model; (b) mathematical constructs of EMIs and DCIs (adapted from Ref. [23])

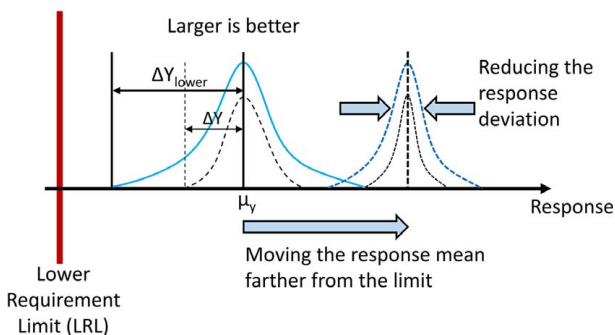


Fig. 4 Achieving a larger value of EMI and DCI

as “satisficing robust solutions” for multiple conflicting goals under uncertainty. A designer’s interest in the cDSP formulation is to minimize the deviation between the targets and what we can achieve for the multiple conflicting goals that best satisfies the individual goal requirements. The goal target values in the robust design cDSP proposed in this paper are target values for EMI and DCI for each goal. This is defined by assigning a value greater than 1 that a designer strives to achieve for each goal but cannot fully meet. A designer can estimate the targets for the EMI and DCI goals by varying the design variables between their limits and checking EMI/DCI responses. This gives a rough estimate. A value higher than that can be defined as a target.

3 The Inverse Decision-Based Design Method for Robust Design Across Process Chains

We define a workflow as a sequence of computational tasks in which information flow from one process/space to another. For

Table 1 The mathematical form of the cDSP with EMI–DCI

cDSP with EMI–DCI for RD Types I, II, III for multiple goals

Given

- n , the number of system variables
- m , the total number of system goals
- $m1$, the number of system goals for robust design Type I, II, and III
- $m2$, the number of system goals for robust design Type I and II
- $m = m1 + m2$
- q , the number of inequality constraints
- $f_{0,i}(x)$, multiple mean response functions
- $f_{1,i}(x)$, multiple upper uncertainty bound functions
- $f_{2,i}(x)$, multiple lower uncertainty bound functions
- $g_{0,i}(x)$, multiple mean constraint functions
- $g_{1,i}(x)$, multiple upper constraint bound functions
- $g_{2,i}(x)$, multiple lower constraint bound functions
- URL_{*i*} and LRL_{*i*}, performance requirements
- Δx , deviations of system variables
- EMI_{Target,*i*}, EMI_{Targets}
- DCI_{Target,*i*}, DCI_{Targets}

Find

- μ_x (mean of system variables)
- d_i^+, d_i^- (deviation variables)

Satisfy

- System constraints:
 - EMI_{constraints,*i*}(x) or DCI_{constraints,*i*}(x) ≥ 1 $i = 1, \dots, q$
 - EMI_{*i*}(x) ≥ 1 $i = 1, \dots, m1$ Robust solution constraints: New constraints defined to ensure
 - DCI_{*i*}(x) ≥ 1 $i = 1, \dots, m2$ robust solutions under multiple conflicting goals
- System goals:
 - EMI_{*i*}(x)/EMI_{Target,*i*} + $d_i^- - d_i^+ = 1$ $i = 1, \dots, m1$
 - DCI_{*i*}(x)/DCI_{Target,*i*} + $d_i^- - d_i^+ = 1$ $i = 1, \dots, m2$
 (assuming there will be at least one goal for EMI and DCI)
- Bounds:
 - $x_i^{\min} \leq x_i \leq x_i^{\max}$ $i = 1, \dots, n$
 - $d_i^-, d_i^+ \geq 0$ and $d_i^+ \cdot d_i^- = 0$ $i = 1, \dots, m$
- Minimize
 - $Z = [f_1(d_i^-, d_i^+), \dots, f_k(d_i^-, d_i^+)]$ Preemptive
 - $Z = \sum W_i(d_i^-, d_i^+), \sum W_i = 1$ Archimedean

the integrated design of materials, products, and associated manufacturing processes, we define two types of workflow, namely, the workflow associated with simulating the behavior of the material through processing–structure–property–performance hierarchy (material workflow) and the workflow associated with the process of design in an inverse manner across process chains (inverse decision workflow). Our focus in this paper is on the uncertainty associated with the inverse decision workflow and the analysis models embodied therein. In Fig. 5, the robust solution space exploration across the process chain considering model structure and model

parameter uncertainty is shown. The method involves two generic steps. To demonstrate the generic nature of the method, we are naming the different sequential spaces as “Space X,” “Space Y,” and “Space Z,” and the decision support constructs as “cDSP i ” and “cDSP $i + 1$.”

Step 1: Establish forward modeling and information flow across Spaces X, Y, and Z

In Step 1, the designer establishes a proper forward flow of information as models are connected across different “Spaces,” thus generating a rough design space. These spaces X, Y, and Z could be the processing–microstructure–property–performance spaces from the materials design standpoint or any sequential model-based transformation of information across spaces/levels in a generic sense. Mathematical models are either identified or developed to establish the information flow. In Fig. 5, Step 1 we see that the output of space serves as the input to the next space and this is repeated to spaces that follow. Thus, Space X (processing space) generates output that serves as an input for Space Y (the microstructure space). The output of Space Y (the microstructure identified) serves as the input for Space Z. The output of Space Z defines the property space, and this directly defines the final performance characteristics of the end product. From a design standpoint, the input to space is design variables and the output response from the space serves as input variables to the next space.

Step 2: Robust solution space exploration across the process chain in an inverse manner (inverse decision workflow)

Step 2.1: Formulate cDSP i for Space Z and carry out solution space exploration

In Step 2, we start the exploration from the rough design space for Space Z (property–performance). In the rough design space, we formulate the decision-based design space for Space Z using the cDSP construct supported by the CEF. This is done in Step 2.1 by formulating cDSP i , see Fig. 5. The decision-based design space thus formulated is represented as the light blue region in Space Z. On exercising cDSP i for the different conflicting goals by assigning preferences, we obtain different solution regions that satisfy individual goals identified by the three circles in Space Z, Fig. 5. If the cDSP is formulated with the robust solution constraint defined in Sec. 2.2.1 (EMI_{*i*}(x) ≥ 1 and DCI_{*i*}(x) ≥ 1), then the regions inside the circle denote the regions with EMI and/or DCI greater than 1 depending on the type of goal formulation. Any region inside the circle satisfies the robust design requirements of that particular goal, and there will be regions with high robustness (high EMI and/or DCI values away from (1) and low robustness (low EMI and/or DCI values that are nearer to (1) within the circle). The designer can pick solutions that achieve maximum robustness for the goal from the solutions. Since the cDSP is formulated with the defined robust solution constraints, such a solution is never reached that gives a high value of EMI and/or DCI for one goal but an EMI and/or DCI less than 1 for another goal, thus ensuring

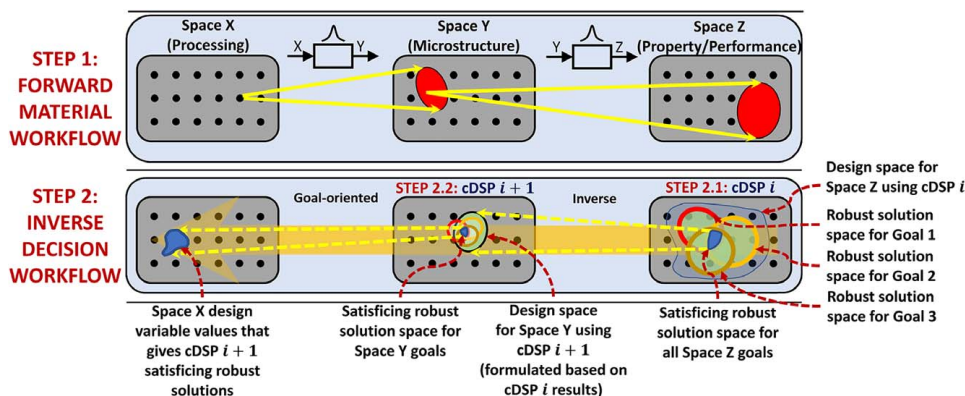


Fig. 5 Robust solution space exploration across the process chain in an inverse manner using the inverse design method

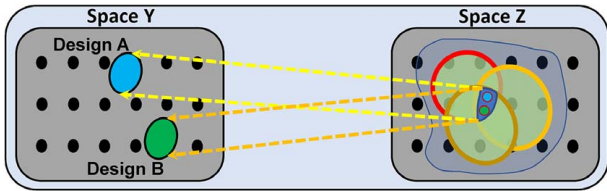


Fig. 6 Designs A and B produce satisfying robust solution space in Space Z

a robust solution space for all the goals. The designer can then explore the robust solution space of all the conflicting goals and identify common robust regions that best satisfy all the goals—satisficing robust solution region for all goals if it exists. This region is identified as the region inside the three circles in Space Z, see Fig. 5. The criteria followed to select the best satisfying robust solution and how this solution is propagated is explained next using the illustration in Fig. 6.

While evaluating the inverse solutions, suppose there exists two design candidates, Design A and Design B, as shown in Fig. 6, for which the corresponding performance spaces in Space Z are either closely similar or exactly identical, then which design should the designer select? Three criteria listed below are used by the designer in this situation and a decision is made based on the evaluation of each of these criteria.

Criterion 1: Which design among Designs A and B best satisfies the designer’s preferences in Space Z?

Criterion 2: Which design among Designs A and B best satisfies the designer’s preferences for Space Y if such a preference exists?

Criterion 3: Which design among Designs A and B best satisfies the designer’s preference for managing the potential uncertainty in the design problem?

Criterion 1 is used when both the designs result in closely similar outcomes but not exactly identical. Criterion 1 is not used when the performance space in Space Z is exactly identical to both the designs as there is no difference in the design outcomes. Criterion 2 is used when the designer has a preference among the solutions A and B as the solutions are further propagated in an inverse manner. Both Criteria 1 and 2 are evaluated based on the designer’s preference for the goals, constraints, and design variable values defined for the problem. Criterion 3 is used to compare the achieved EMI and/or DCI values for both the designs A and B and then evaluate the most robust solution among those. Solutions with higher EMI and/or DCI values are better in terms of management of potential uncertainty in the design problem. All these criteria are evaluated by the designer, and a decision is made among Designs A and B that best meets the designer’s requirements. Once the design for Space Y is identified, a new cDSP (cDSP $i + 1$) is formulated in Space Y to achieve the identified design targets as closely as possible.

Step 2.2: Formulate cDSP $i + 1$ for Space Y and carry out solution space exploration

Once cDSP i is executed and satisficing robust solution region is identified, cDSP $i + 1$ for Space Y is formulated. This cDSP is formulated with design variable values identified from first cDSP as the Space Y goal requirements and is formulated in terms of EMI and/or DCI depending on the type of uncertainty present (the circle with the green region in Space Y represents the region identified from the previous cDSP and is the design space for the new cDSP, see Fig. 5). On solving the cDSP with EMI–DCI for Space Y and exploring the solution space, we obtain the robust solution regions that satisfy each goal (represented by the three circles inside the green region in Space Y, see Fig. 5). From these robust solutions, the designer identifies the satisficing robust region for all the goals—the blue region within the circles. The values of the Space X design variables that give this robust satisficing Space Y region are identified based on the cDSP $i + 1$ results (the blue region in the Space X, see Fig. 5).

Thus, using this proposed method, the designer is able to carry out decision-based robust design exploration of Spaces X, Y, and Z in an inverse manner. An application as discussed could be the identification of material processing paths and microstructure to satisfy a ranged set of product-level performance requirements. However, the method is generic and can be applied to other complex system problems involving sequential model-based flow of information under uncertainty. The characteristics of the problems for which the method can be applied include: (i) sequential model-based information transformation from one space to another, (ii) availability of analytical models for responses as a function of control and noise factors, and (iii) availability of information on model parameter and model structure uncertainty. In Sec. 4, we demonstrate the efficacy of the method and the associated robust design functionalities using an industry-inspired hot rolling and cooling process chain example problem for the production of a steel rod.

4 Test Example: Robust Concept Exploration of Material (Steel), Product (Rod), and Associated Manufacturing Processes (Hot Rolling and Cooling)

Developing new grades of steels with improved properties and performances is the focus of steel manufacturers. Developing steels with a range of mechanical properties resulting in improved performance of products is possible by carefully managing the material processing and thereby tailoring the microstructure generated. Several manufacturing processes such as casting, reheating, rolling, and cooling are involved in the processing of a steel rod. This round rod produced is further used for gear production after forging into gear blanks. The end properties of the rolled product are influenced by the chemical composition of the steel including the segregation of alloying elements, the deformation history during rolling, the cooling after rolling and the microstructure generated after rolling and cooling processes. The steel rod-making process chain is highly complex due to large numbers of design variables, constraints and bounds, conflicting goals, and sequential information/material flow during material processing. Many plant trials that are usually expensive and time-consuming are required to produce a new steel grade with desired properties and performance. An alternative, therefore, is to carry out simulation-based, integrated design exploration of the different manufacturing processes involved by exploiting the advances in computational modeling and identifying a ranged set of robust solutions that satisfy the requirements of the processes and product.

In Fig. 7, we show the process–structure–property–performance hierarchy for the integrated design of hot rolling and cooling processes to produce the steel rod. Using Fig. 7, we capture the forward material workflow for the problem. The processing stage involves the two manufacturing processes, namely hot rolling and cooling. During hot rolling, the thermo-mechanical processing of the material happens. The modeling of the hot rolling process involves a hot deformation module, recrystallization module, grain growth module, and flow stress module [36]. The inputs to the rolling process are the chemical composition, initial austenite grain size after reheating, and the rolling schedule (strain, strain rate, interpass time, and number of passes). Using these inputs, we predict the temperature evolution, flow stress and calculate the final austenite grain size (AGS, D) after rolling, see Ref. [36]. In our design problem, we are interested in the final AGS and it forms the input from rolling side to the microstructure space. The microstructure space is generated during the cooling process. During the cooling process, depending on the cooling rate (CR) and the final AGS from rolling and the chemical composition of the incoming steel, time-temperature transformations and simultaneous transformations take place. This results in the phase transformation of austenite to different steel phases like Allotriomorphic ferrite, Widmanstatten ferrite, pearlite, etc. Also, alternate layers of the banded microstructure of ferrite and pearlite can also form

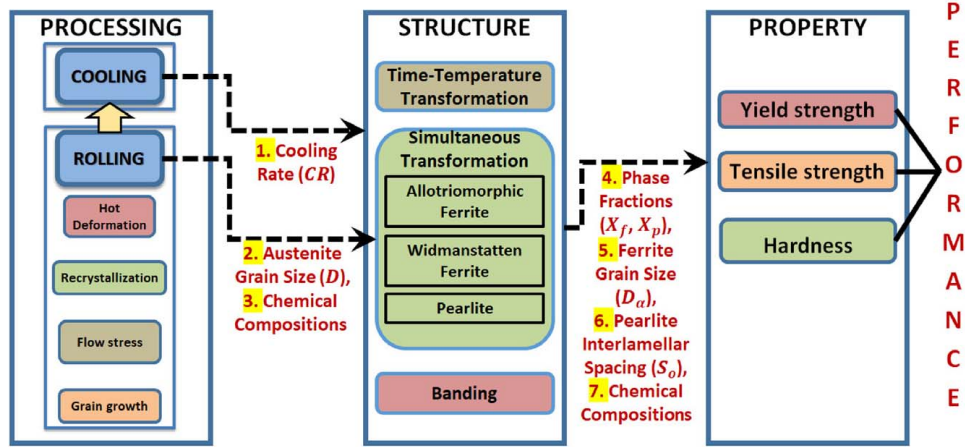


Fig. 7 Process–structure–property–performance hierarchy for the integrated design of hot rolling and cooling processes to produce a steel rod—forward material workflow

depending on the micro-segregates that are present and the cooling conditions. In our design study, we consider the transformations of austenite to ferrite and pearlite. The output after the cooling process from the microstructure space as shown in Fig. 7 is the phase fractions of ferrite and pearlite (X_f and X_p), ferrite grain size (FGS) after transformation (D_f), pearlite interlamellar spacing (S_o), and the chemical composition of the material. These serve as an input for the property space to predict the mechanical properties, the yield strength, tensile strength, and hardness which are measures of performance for the final rod product. This completes the forward material workflow for the problem we are addressing and establishes the process–structure–property–performance hierarchy for the material system. In Secs. 4.1 and 4.2, we discuss the Steps 1 and 2 of the proposed method.

4.1 Step 1: Establish Forward Modeling and Information Flow Across the Process Chain (Material Workflow)

4.1.1 Identifying Factors (Input) and Responses Across Process Chain (See Steps of Concept Exploration Framework). For the hot rod rolling process chain problem addressed in this paper, the mechanical property goals and requirements are for yield strength (YS), tensile strength (TS), and hardness (HV). These mechanical properties are dependent on the final microstructure after cooling like the ferrite grain size after cooling (FGS, D_f), the phase fractions of ferrite (X_f) and pearlite ($1 - X_f$), the pearlite interlamellar spacing (S_o), and the composition variables like silicon [Si], nitrogen [N], phosphorous [P], and manganese [Mn]. These microstructure factors are defined by the rate (CR) at which cooling is carried out and the final austenite grain size after rolling (AGS, D) and composition variables like carbon [C] and manganese [Mn].

4.1.2 Identify Models and Relationships That Map From Processing Space to Final Performance Space Across the Process Chain Taking Into Account the Uncertainty in Models and Design Variables

4.1.2.1 Microstructure–mechanical property correlation models. The mechanical properties for the end rod produced are represented by yield strength (YS), tensile strength (TS), and hardness (HV). Gladman et al. [29,30] were instrumental in predicting the mechanical properties of plain carbon steel products as a function of the microstructural parameters of the ferrite–pearlite microstructure. Models were later developed by Hodgson and Gibbs [37], Majta et al. [27], and Kuziak et al. [28].

4.1.2.2 Models for yield strength and the variability associated. Over the years, different researchers have predicted yield strength as a function of different microstructural parameters. These different models when used to predict values at different ranges for a given input and hence have variability associated with them in the prediction of the yield strength property. In this paper, to demonstrate our method for inverse design and managing uncertainty, we assume the yield strength model by Gladman et al. [29,30] as the mean response model $f_0(x)$ for our problem. The upper uncertainty bound function $f_1(x)$ for yield strength is the model by Hodgson and Gibbs [37] that when used always predicts yield strength higher than the model by Gladman and coauthors for a given input. The lower uncertainty bound function $f_2(x)$ for yield strength is the model by Kuziak et al. [28] that when used to predicts yield strength at a lower level than the mean response model for a given input. The models thus identified for yield strength are

$$\begin{aligned} \text{Yield strength} & & \text{YS}_{f_0(x)} &= 63[\text{Si}] + 425[\text{N}]^{0.5} + X_f^{1/3}(35 + 58[\text{Mn}] + 17(0.001D_f)^{-0.5}) \\ \text{(mean response function)} & & & + (1 - X_f^{1/3})(179 + 3.9S_o^{-0.5}) \end{aligned} \quad (9)$$

$$\begin{aligned} \text{Yield strength} & & \text{YS}_{f_1(x)} &= 62.6 + 26.1[\text{Mn}] + 60.2[\text{Si}] + 759[\text{P}] \\ \text{(upper uncertainty bound function)} & & & + 212.9[\text{Cu}] + 3286[\text{N}] + 19.7(0.001D_f)^{-0.5} \end{aligned} \quad (10)$$

$$\begin{aligned} \text{Yield strength} & & \text{YS}_{f_2(x)} &= X_f(77.7 + 59.9 \times [\text{Mn}] + 9.1 \times (0.001D_f)^{-0.5}) \\ \text{(lower uncertainty bound function)} & & & + 478[\text{N}]^{0.5} + 1200[\text{P}] + (1 - X_f)[145.5 + 3.5S_o^{-0.5}] \end{aligned} \quad (11)$$

The mean response function and prediction interval models are plotted as shown in Fig. 8. The models are depicted as a function of the ferrite grain size (FGS, D_α) and ferrite fraction (X_f) for a value of pearlite interlamellar spacing of 0.15 (μm), manganese concentration of 1.5 (%), nitrogen of 0.007 (%), silicon of 0.36 (%), phosphorous of 0.019 (%), and copper of 0.08 (%).

4.1.2.3 Model for tensile strength. We select the model by Kuziak and coauthors, in which they describe the tensile strength TS, of carbon–manganese steels as a function of ferrite grain size after cooling D_α , cooling rate CR , ferrite fraction X_f , the pearlite interlamellar spacing S_o , and the composition elements in the steel [28], see Eq. (12).

$$\text{TS} = X_f(20 + 2440 \times [\text{N}]^{0.5} + 18.5 \times (0.001D_\alpha)^{-0.5}) + 750(1 - X_f) + 3(1 - X_f^{0.5})S_o^{-0.5} + 92.5 \times [\text{Si}] \quad (12)$$

4.1.2.4 Model for hardness. Hardness (HV) is represented as a function of ferrite and pearlite fractions, average austenite to ferrite transformation temperature (T_{mf}), and the weight percentage of silicon (Si) based on the investigation by Yada [31], see Eq. (13).

$$\text{HV} = X_f(361 - 0.357T_{mf} + 50[\text{Si}]) + 175(1 - X_f) \quad (13)$$

4.1.3 Processing-Microstructure Correlation Models

4.1.3.1 Model for ferrite fraction. We select the response surface model developed by Nellippallil et al. [25] for ferrite fraction, see Eq. (14). The model is developed by carrying out a design of experiments using the program STRUCTURE developed by Jones and Badeshia to predict the simultaneous transformation of austenite.⁴ For more details on the development of the response surface model and the validation of the same, see Refs. [38–41].

$$X_f = 1 - \left(\begin{array}{l} 0.206 - 0.117[\text{Mn}] - 0.0005CR - 0.00113D \\ + 0.248[\text{C}] + 0.00032[\text{Mn}]CR \\ + 0.000086[\text{Mn}]D + 0.9539[\text{Mn}][\text{C}] \\ - 4.259 \times 10^{-6}CR * D \\ + 0.00726CR[\text{C}] + 0.0023D[\text{C}] \\ - 0.0305[\text{Mn}]^2 - 0.0000056CR^2 \\ + 4.859 \times 10^{-6}D^2 + 0.79[\text{C}]^2 \end{array} \right) \quad (14)$$

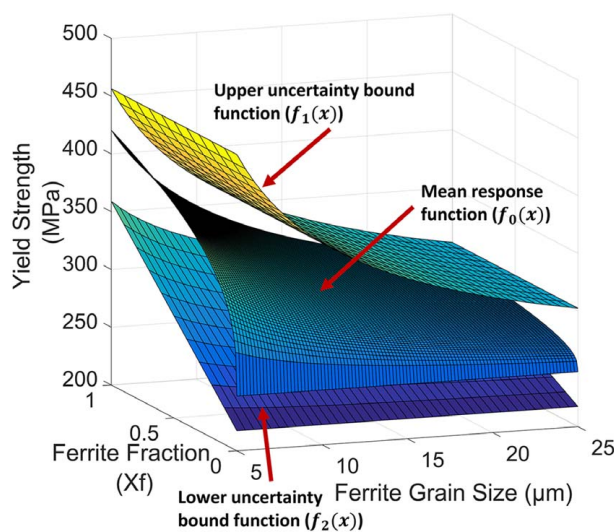


Fig. 8 The mean response function and the upper and lower uncertainty bound functions for yield strength

⁴<http://www.msm.cam.ac.uk/map/steel/programs/structure.html>.

4.1.3.2 Model for ferrite grain size. We select the model by Hodgson and Gibbs [37] for defining ferrite grain size, see Eq. (15). The factors affecting ferrite grain size D_α are final austenite grain size after rolling D , retained strain ϵ_r , the composition of carbon and manganese measured in terms of carbon equivalent C_{eq} , and cooling rate CR from the cooling side.

$$D_\alpha = (1 - 0.45\epsilon_r^{0.5}) \times \{(-0.4 + 6.37C_{eq}) + (24.2 - 59C_{eq})CR^{-0.5} + 22[1 - \exp(0.015D)]\} \quad (15)$$

where $C_{eq} = (C + \text{Mn})/6$

4.1.3.3 Model for pearlite interlamellar spacing. We select the model by Kuziak et al. [28] where pearlite interlamellar spacing S_o is defined as a function of carbon C, manganese Mn, and cooling rate CR , see Eq. (16).

$$S_o = 0.1307 + 1.027[\text{C}] - 1.993[\text{C}]^2 - 0.1108[\text{Mn}] + 0.0305CR^{-0.52} \quad (16)$$

4.2 Step 2: Carry Out Inverse Decision-Based Robust Design Exploration

4.2.1 Step 2.1: Robust Solution Space Exploration of Property–Performance Space. We start the inverse decision-based robust design exploration from property–performance space. The cDSP for the last space is formulated with EMI and DCI goals that capture both property and performance requirements for the end product. The design variables for this cDSP will be the output responses from Microstructure space which forms the input for property–performance space, see Fig. 7. On exercising the cDSP, the process designer will be able to solve and capture the knowledge associated with the following inverse problem: *Given the end mechanical properties of a new steel product mix, what should be the microstructure factors after phase transformation that satisfies the requirements identified taking into account the uncertainty associated with models and parameters associated?* The cDSP reads as follows:

cDSP for Property–Performance (Larger is Better)

Given

End requirements identified for the rod rolling process

- maximize yield strength;
- maximize tensile strength; and
- maximize hardness.

$f_{0,i}(x)$, multiple mean response functions, $f_{1,i}(x)$, multiple upper uncertainty bound functions, and $f_{2,i}(x)$, multiple lower uncertainty bound functions. $\text{LRL}_{\text{YS}} = 200 \text{ MPa}$, $\text{LRL}_{\text{TS}} = 450 \text{ MPa}$ and $\text{LRL}_{\text{HV}} = 130$.

$\text{EMI}_{\text{Target,YS}} = 3 \text{ EMI}_{\text{Target}}$ for EMI goal for YS considering Types I, II, and III robust design (RD); $\text{DCII}_{\text{Target,TS}} = 8 \text{ DCI}_{\text{Target}}$ for DCI goal for TS considering Types I and II RD; and $\text{DCII}_{\text{Target,HV}} = 8 \text{ DCI}_{\text{Target}}$ for DCI goal for HV considering Types I and II RD

System variables, their ranges, and variability

Fixed parameters

Composition elements	Concentration (%)
C	0.18
Si	0.36
V	0.003
Cu	0.08
N	0.007
P	0.019

Find

μ_x (mean location of system variables)

Deviation variables

$$d_i^-, d_i^+, \quad i = 1, 2, 3$$

Satisfy**System constraints**

- Robust solution constraint for YS
 $EMI_{YS}(x) \geq 1$
- Robust solution constraint for TS
 $DCI_{TS}(x) \geq 1$
- Robust solution constraint for HV
 $DCI_{TS}(x) \geq 1$

System goals**Goal 1:**

- Maximize EMI for yield strength

$$\frac{EMI_{YS}(x)}{EMI_{Target, YS}} + d_1^- - d_1^+ = 1$$

$$\text{where } EMI(x) = \{f_0(x) - LRL\} / \{Y_{min} - f_0(x)\}$$

$$\text{where } Y_{min} = \min \left\{ \left(f_j(x) - \sum_{i=1}^n \left| \frac{\partial f_j}{\partial x_i} \right| \cdot \Delta x_i \right) \right\}$$

Goal 2:

- Maximize DCI for tensile strength

$$\frac{DCI_{TS}(x)}{DCI_{Target, TS}} + d_2^- - d_2^+ = 1$$

Goal 3:

- Maximize DCI for hardness

$$\frac{DCI_{HV}(x)}{DCI_{Target, HV}} + d_3^- - d_3^+ = 1$$

$$\text{where } DCI(x) = \{f_0(x) - LRL\} / \Delta Y$$

$$\text{where } \Delta Y = \sum_{i=1}^n \left| \frac{\partial f_0}{\partial x_i} \right| \Delta x_i$$

Variable bounds

Defined in Table 2

Bounds on deviation variables

$$d_i^-, d_i^+ \geq 0 \text{ and } d_i^- * d_i^+ = 0, \quad i = 1, 2, 3$$

Minimize

We minimize the deviation function

$$Z = \sum_{i=1}^3 W_i (d_i^- + d_i^+), \quad \sum_{i=1}^3 W_i = 1$$

On exercising the cDSP for different design scenarios and carrying out robust solution space exploration, following the steps in Concept Exploration Framework, we obtain the combinations for D_α , X_f , S_0 , and Mn that best satisfy the end mechanical properties

Table 2 System variables, ranges, and variability

Sr. No	System variables (X)	Ranges	Variability (Δx)
1	X_1 , ferrite grain size (D_α)	5–25 μm	[± 3]
2	X_2 , the phase fraction of ferrite (X_f)	0.1–1	[± 0.1]
3	X_3 , the pearlite interlamellar spacing (S_0)	0.15– 0.25 μm	[± 0.01]
4	X_4 , manganese concentration after cooling ([Mn])	0.7–1.5%	[± 0.1]

in the presence of model structure and model parameter uncertainty. The desired solution ranges identified for D_α , X_f , and S_0 are then identified as the target goals for the next cDSP (cDSP for microstructure space).

We exercise 13 different scenarios for the cDSP formulated in Sec. 4.2 using the computational infrastructure DSIDES [42]. Different weights are assigned to each goal in these scenarios. Details of the scenarios and the results obtained for the goals are provided in Table 3.

These scenarios are selected based on judgment to effectively capture the design space for exploration in a ternary space with the different combination of weights on goals. Next, we explain the significance of each of these scenarios and identify robust satisfying solutions from the solution space generated in Table 3. We explain the significance of the scenarios using the cDSP for the property–performance space. Scenarios 1–3 are for a situation where the designer's interest is to achieve the target of one of the goals, maximizing EMI_{YS} , maximizing DCI_{TS} , or maximizing DCI_{HV} as close as possible. For example, the designer's preference in Scenario 3 is to achieve only the DCI goal for hardness. Scenarios 4–6 are for a situation where two goals are given equal preference, while the third goal is not given any preference. For example, Scenario 5 is a situation where the designer's interest is in equally maximizing EMI_{YS} and DCI_{HV} without giving any preference to the DCI_{TS} goal. Scenarios 7–12 are situations where the designer gives greater preference to one goal, a lesser preference to the second goal, and zero preference to the third goal. Scenario 13 is a situation where the designer gives equal preference to all the three goals considered. The exploration of solution space is carried out by exercising the cDSPs for these scenarios using DSIDES and plotting the solution space obtained in a ternary space. In the context of our work, the axes of the ternary plots are the weights assigned to each goal, and the color contour in the interior is the achieved value of the specific goal that is being addressed. From these plots, we identify feasible solution regions that satisfies our requirements and the associated weights to be assigned to each goal to achieve this solution space. More details on the creation and interpretation of ternary plots are available in Ref. [43].

In Figs. 9(a)–9(c), we show via the ternary plots the achieved values of yield strength (Goal 1), tensile strength (Goal 2), and hardness (Goal 3), respectively, for all the 13 scenarios. For Goals 1, 2, and 3, we are interested in achieving high values of EMI_{YS} , DCI_{TS} , and DCI_{HV} , respectively. We see from Figs. 9(a)–9(c) that the solution spaces are composed of solutions with $EMI_{YS} \geq 1$, $DCI_{TS} \geq 1$, and $DCI_{HV} \geq 1$, respectively. This ensures robust solutions under both model structure and model parameter uncertainty for Goal 1, and robust solutions under model parameter uncertainty for Goals 2 and 3. The maximum EMI_{YS} , DCI_{TS} , and DCI_{HV} are achieved in the red regions, and these regions are therefore the most robust regions. The dark blue regions are the least robust in the solution spaces generated. We define acceptable compromised robust regions within the solution spaces as $EMI_{YS} \geq 1.5$, $DCI_{TS} \geq 6$, and $DCI_{HV} \geq 7$ identified by the dashed lines. Any solution points lying within these regions are acceptable for us as these points satisfy the requirement for the three goals under uncertainty.

Since we are interested in identifying *satisficing robust solution* regions for the multiple conflicting goals, we plot the superposed plot with all the robust solution spaces of interest as shown in Fig. 10. The light-yellow region identified in Fig. 10 satisfies the robust design requirements identified for the conflicting mechanical property goals. In Fig. 10, we highlight three points A, B, and C. A is the most robust region for YS with high EMI but lowest for TS and HV with low DCIs. Similarly, B is the most robust region for TS with high DCI_{TS} but lowest for YS with low EMI_{YS} . Point C (Scenario 13 in Table 3) lying inside the satisfying robust solution space achieves the highest DCI_{HV} and is the most robust region for HV goal satisfying the robust design requirements of other goals. We select Point C and the solution region around it as the robust solution of interest, and this information is passed to the cDSP for microstructure space (Table 4).

Table 3 Scenarios and achieved values of goals

Scenarios	w1	w2	w3	Goal 1—EMI _{YS}	Goal 2—DCI _{TS}	Goal 3—DCI _{HV}
1	1	0	0	2.635684224	1.000026749	2.650971569
2	0	1	0	1.202283838	8.110528422	8.663291569
3	0	0	1	1.226883558	7.450292555	8.278751569
4	0.5	0.5	0	1.570932001	6.818501827	8.691461569
5	0.5	0	0.5	1.663214956	5.852196386	7.748441569
6	0	0.5	0.5	1.188246479	8.154843742	8.640151569
7	0.25	0.75	0	1.408711494	7.277846111	8.786341569
8	0.25	0	0.75	1.663636535	5.847812704	7.744171569
9	0.75	0	0.25	1.673002166	5.769498377	7.668461569
10	0.75	0.25	0	1.584223565	6.7201117931	8.596961569
11	0	0.75	0.25	1.202283838	8.110528422	8.663291569
12	0	0.25	0.75	1.192159649	8.146318646	8.647991569
13	0.34	0.33	0.33	1.562131147	6.917735445	8.786341569

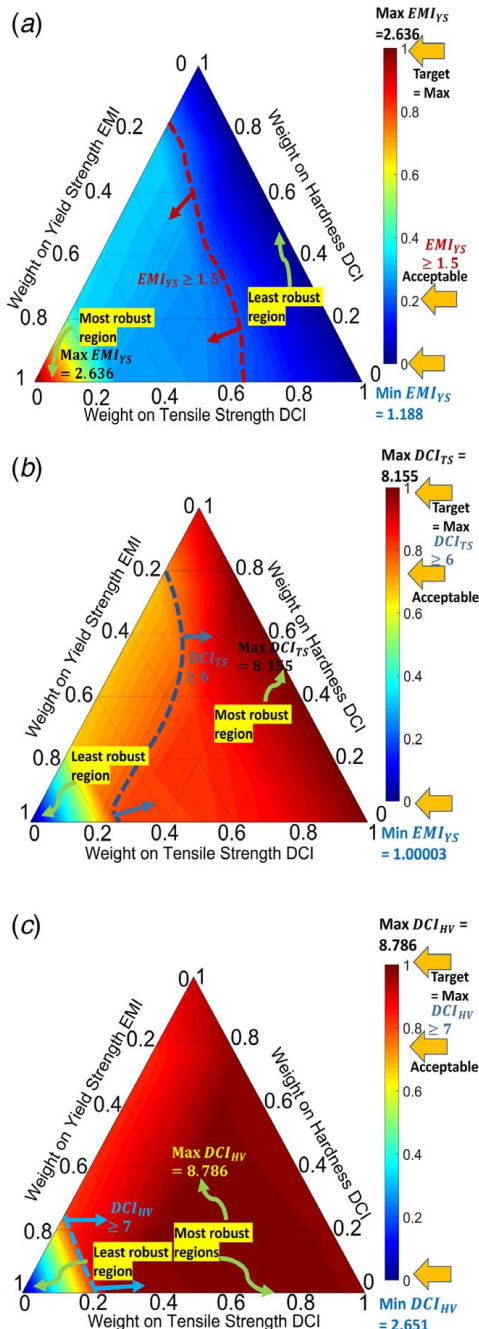


Fig. 9 Robust solution space for (a) YS, (b) TS, and (c) HV

4.2.2 Step 2.2: Carry Out Inverse Decision-Based Design Exploration of Microstructure Space. We carry out the inverse decision-based design exploration of microstructure space with information coming from the first cDSP as our requirements. The three goals for X_f , D_α , and S_0 are defined with the designer's interest to achieve the values identified in Table 4 as close as possible. Upper requirement limits ($URL_{X_f}=0.75$, $URL_{D_\alpha}=30\mu\text{m}$, $URL_{S_0}=0.2\mu\text{m}$) for the three goals are defined since the individual goal requirements are to achieve as small value as possible (smaller is the better case). In this formulation, we are considering only the model parameter uncertainty with an assumption that the model structure uncertainty does not exist. The cDSP for the microstructure space is thus formulated with the DCI goals that captures microstructure requirements identified under model parameter uncertainty. The design variables for this cDSP will be the output responses from the processing space which forms the input for microstructure space, see Fig. 7. The cDSP with DCI reads as follows:

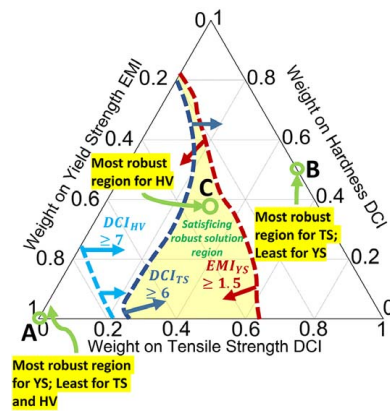


Fig. 10 Superposed robust solution spaces

Table 4 Microstructure information for next cDSP

Sol. Pt	Microstructure factors (solutions identified are passed as microstructure requirements to next cDSP)				Mechanical properties of rod (achieved robust values)		
	X_f	D_α (μm)	S_0 (μm)	Mn (%)	YS (MPa)	TS (MPa)	HV
C	0.1 (± 0.1)	24.7 (± 3)	0.15 (± 0.01)	0.7 (± 0.1)	245	747	170

4.2.2.1 *Compromise design support problem for microstructure space (smaller is better), robust designs I and II.*
Given

End requirements identified for the rod rolling process are as follows

- Minimize ferrite fraction;
- Minimize ferrite grain size; and
- Minimize pearlite interlamellar spacing.

$f_{0,i}(x)$, multiple mean response functions

$$\text{URL}_{X_f} = 0.75$$

$$\text{URL}_{D_\alpha} = 30\mu\text{m}$$

$$\text{URL}_{S_o} = 0.2\mu\text{m}$$

$\text{DCI}_{\text{Target}, X_f} = 10$, $\text{DCI}_{\text{Target}, D_\alpha} = 10$, and $\text{DCI}_{\text{Target}, S_o} = 200$.
 System variables, their ranges, and variability

Find

μ_x (mean location of system variables)

Deviation variables

$$d_i^-, d_i^+, \quad i = 1, 2, 3$$

Satisfy

System constraints

- Robust solution constraint for ferrite fraction

$$\text{DCI}_{X_f}(x) \geq 1$$

- Robust solution constraint for ferrite grain size

$$\text{DCI}_{D_\alpha}(x) \geq 1$$

- Robust solution constraint for Pearlite Interlamellar spacing

$$\text{DCI}_{S_o}(x) \geq 1$$

System goals

Goal 1:

- Maximize DCI for ferrite fraction

$$\frac{\text{DCI}_{X_f}(x)}{\text{DCI}_{\text{Target}, X_f}} + d_1^- - d_1^+ = 1$$

Goal 2:

- Maximize DCI for ferrite grain size

$$\frac{\text{DCI}_{D_\alpha}(x)}{\text{DCI}_{\text{Target}, D_\alpha}} + d_2^- - d_2^+ = 1$$

Goal 3:

- Maximize DCI for pearlite interlamellar spacing

$$\frac{\text{DCI}_{S_o}(x)}{\text{DCI}_{\text{Target}, S_o}} + d_1^- - d_1^+ = 1$$

$$\text{where } \text{DCI}(x) = \{\text{URL} - f_0(x)\} / \Delta Y$$

$$\text{where } \Delta Y = \sum_{i=1}^n \left| \frac{\partial f_0}{\partial x_i} \right| \Delta x_i$$

Variable bounds

Defined in Table 5

Bounds on deviation variables

$$d_i^-, d_i^+ \geq 0 \text{ and } d_i^- * d_i^+ = 0, \quad i = 1, 2, 3$$

Table 5 System variables, ranges, and variability

Sr. No	System variables (X)	Ranges	Variability (Δx)
1	X_1 , Cooling rate (CR)	11–100 K/min	(± 10)
2	X_2 , Austenite grain size (D)	30–100 μm	(± 10)

Minimize

We minimize the deviation function

$$Z = \sum_{i=1}^3 W_i (d_i^- + d_i^+), \quad \sum_{i=1}^3 W_i = 1$$

On exercising the cDSP for different design scenarios and carrying out robust solution space exploration, following the steps in the Concept Exploration Framework, we obtain the combinations for CR and D, the variables from processing space that best satisfy the microstructure requirements in the presence of model parameter uncertainty. The cDSP formulated for microstructure space is exercised for 13 different scenarios (the same scenarios as given in Table 3) by assigning weights to the goals using DSIDES.

In Figs. 11(a)–11(c), we show the robust solution space for ferrite fraction, X_f (Goal 1), D_α (Goal 2), and S_o (Goal 3), respectively. Our interests in Goals 1, 2, and 3 are to achieve high DCI values for X_f , D_α , and S_o , respectively. The ternary spaces are made of $\text{DCI}_{X_f} \geq 1$, $\text{DCI}_{D_\alpha} \geq 1$, and $\text{DCI}_{S_o} \geq 1$, ensuring robust solutions under model parameter uncertainty associated with the design variables. We compromise and identify the regions with $\text{DCI}_{X_f} \geq 7$, $\text{DCI}_{D_\alpha} \geq 9.5$, and $\text{DCI}_{S_o} \geq 150$ as the robust satisfying regions of interest under uncertainty as shown in Fig. 11.

To identify satisfying robust solution regions for microstructure, we plot the superposed plot shown in Fig. 12 with all the robust solution spaces of interest. In the superposed ternary plot, we see that the light-yellow region satisfies all the identified microstructure requirements under model parameter uncertainty. To analyze further we pick three solution points from the region identified. Solution points A, B, and C lie within the region that satisfies all the robust design goals in the best possible manner. The results associated with the selected points are summarized in Table 6.

On analyzing the results in Table 6, we see that the solutions identified from the satisfying robust region in the ternary space show a very small deviation in performance from each other. The processing variable values associated with the solution points in this region results in robust solutions of microstructure under the model parameter uncertainty considered in this design problem.

Thus, using this proposed inverse method, we are able to carry out top-down driven, decision-based robust design exploration of processing paths and material microstructure to satisfy a ranged set of product-level performance requirements. The inverse method proposed is generic and can be applied to similar problems with information flow from one process to another to design the system under different types of uncertainty classified in this paper.

5 Discussion: Robustness Under Model Structure and Model Parameter Uncertainty Using Error Margin Indices and Design Capability Indices

In this section, based on the design study carried out, we discuss the usefulness of the robust design metrics EMI and DCI used in this paper for designing a system under model structure and model parameter uncertainty by carrying out a comparative study. To illustrate the same, we use the yield strength model proposed by Gladman and coauthors (Eq. (9)), which we used as the mean response function for YS in the cDSP formulated for property–performance space. We explore three formulations: In the first, we formulate a single goal cDSP with an EMI for the yield strength mean model with the uncertainty bounds defined by the yield strength

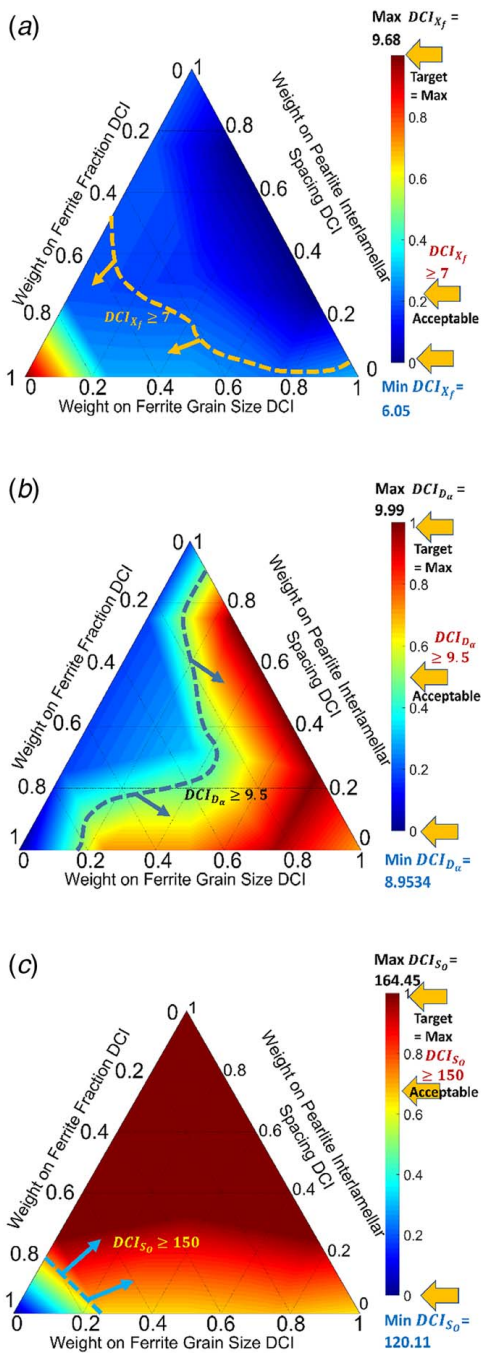


Fig. 11 Robust solution space for (a) X_f , (b) D_a , and (c) S_0

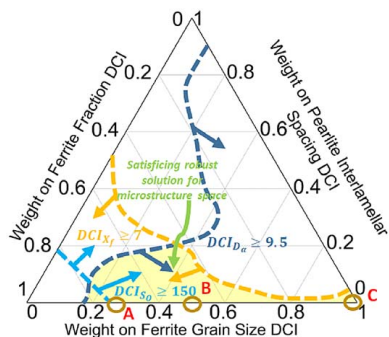


Fig. 12 Superposed robust solution spaces

Table 6 Solution points selected

Sol. Pts	Factors from processing space		Microstructure space		
	CR (K/min)	D (μm)	X_f	D_a (μm)	S_0 (μm)
A	94	46	0.69147	13.1038	0.176
B	93.9	46.	0.691	13.103	0.1763
C	93.7611	45.7	0.69125	13.0554	0.1763

models by Hodgson and Gibbs (Eq. (10)) and Kuziak and coauthors (Eq. (11)); the formulation is the same as in the first cDSP, except there is only one goal which is for maximizing the EMI for yield strength). In the second, we formulate a single goal cDSP with a DCI goal for the yield strength mean model in consideration of only model structure uncertainty defined in the first cDSP. Third, we formulate a single-objective traditional optimization problem for maximizing the mean yield strength function.

The results associated with this comparative study are plotted in Fig. 13 with ferrite fraction and ferrite grain size as the input factors for the yield strength model. We see that the cDSP with EMI predicts a mean response value of 288.755 MPa. The corresponding EMI value for the solution point is 2.63568. The formulation with DCI predicts yield strength at 306.08 MPa and is higher than that with the EMI prediction. The DCI value at this point is 5.37195. However, the EMI value when calculated is only 1.85375. This means that the EMI is less for the solution point that is identified using DCI formulation compared to the solution point identified using an EMI formulation. This is because the DCI formulation overlooks the uncertainty associated with the model and thus achieves a lower EMI value for the design solutions. Next, by analyzing the solution obtained via the single-objective optimization formulation, we see that the optimal solution predicts the highest response for yield strength ($YS = 420.654$ MPa). However, both the DCI and EMI values are low for the optimization solution point when calculated. This means that the optimal solution points obtained are prone to both model structure and model parameter uncertainty and are less robust compared with the solutions obtained via cDSP-DCI and cDSP-EMI.

We infer from this comparative study, the advantage of EMI and DCI formulations for complex material-product and process systems as the design solutions are more robust against model structure uncertainty and model parameter uncertainty. The limitation here with the EMI and DCI is the inability to capture the designer's preference since the EMI and DCI are calculated as a combination of mean and response variations. This limitation can be overcome by separating the mathematical combinations of mean and

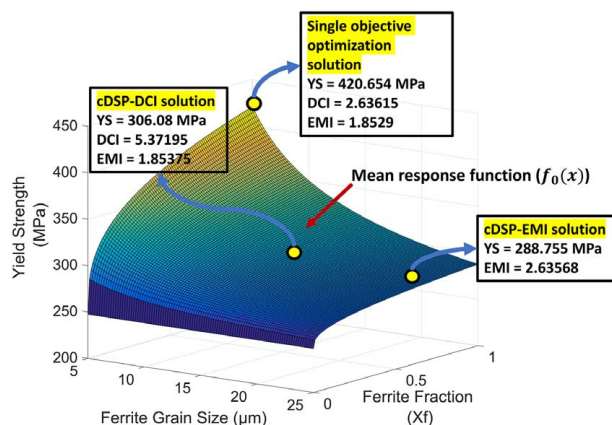


Fig. 13 Solutions obtained for yield strength as a single goal using different formulations—a comparative study

performance variance and formulating them as two individual goals in the cDSP and repeating the same for multiple goals.

6 Closing Remarks

In this paper, we present a robust concept exploration by extending the goal-oriented inverse design method proposed by Nellippallil et al. [25] to identify *satisficing robust solutions* across process chains. The extension embodies the introduction of specific robust design goals and new robust solution constraints anchored in the mathematical constructs of EMIs and DCIs to determine “satisficing” robust design specifications for multiple conflicting goals from the standpoint of Types I, II, and III robust design across process chains. The utility of the proposed method, robust design goals, constraints, and metrics proposed is demonstrated by carrying out the solution space exploration of the processing and microstructure spaces of the rolling and cooling processes to identify *satisficing robust solutions* to realize the end mechanical properties of the rod product. The contributions in this paper are the following:

- (1) The previous work by Choi et al. [23] on robust design using EMI address only a single-objective case. In this paper, we address multiple conflicting goals and how satisficing robust solutions can be explored across a process chain using the inverse design method.
- (2) We make it possible for a designer to handle multiple robust design formulations (using both EMI and DCI) in one problem formulation. This allows designers to look at robust design Types I and II for one goal (via DCI) and Types I, II, and III for another goal (via EMI) in a single problem formulation depending on the problem requirements.

Based on these contributions, the key functionalities of the GoID method with robust design metrics, goals, and constraints when compared to other domain-independent design exploration methods include the following:

- an increase in the problem size as there are no limitations in the number of design variables and goals to be studied,
- improved flexibility in the design of the various processes involved as individual design spaces are formulated at each level allowing designers to incorporate new design goals and requirements;
- the capability to identify robust satisficing solutions for multiple conflicting goals under multiple sources of uncertainty; and
- the capability to visualize and explore solutions that are relatively insensitive to the sources of uncertainty identified.

The method and associated robust design constructs are generic and can be applied to coordinate information flow and human decision-making across processes/levels in order to realize an end goal by managing the sources of uncertainty—a key functionality that allows the application of this method to other complex system problems involving sequential model-based flow of information under uncertainty.

Acknowledgment

The authors thank Tata Consultancy Services Research, Pune, for supporting this work (Grant No. 105-373200). Janet K. Allen and Farrokh Mistree gratefully acknowledge the financial support from the John and Mary Moore and the L.A. Comp Chairs at the University of Oklahoma, respectively.

References

[1] Ashby, M. F., and Cebon, D., 1993, “Materials Selection in Mechanical Design,” *Le Journal de Physique IV*, 3(C7), pp. C7-1–C7-9.

[2] Norton, R. L., 1996, *Machine Design: An Integrated Approach*, Prentice-Hall Inc., NJ.

[3] Shigley, J. E., 1972, *Mechanical Engineering Design*, McGraw-Hill, New York.

[4] Pahl, G., and Beitz, W., 2013, *Engineering Design: A Systematic Approach*, Springer Science & Business Media, London.

[5] Olson, G. B., 1997, “Computational Design of Hierarchically Structured Materials,” *Science*, 277(5330), pp. 1237–1242.

[6] McDowell, D. L., Panchal, J., Choi, H.-J., Seepersad, C., Allen, J., and Mistree, F., 2009, *Integrated Design of Multiscale, Multifunctional Materials and Products*, Butterworth-Heinemann, Waltham, MA.

[7] Horstemeyer, M. F., 2018, *Integrated Computational Materials Engineering (ICME) for Metals: Concepts and Case Studies*, John Wiley & Sons, Hoboken, NJ.

[8] McDowell, D. L., 2018, “Microstructure-Sensitive Computational Structure-Property Relations in Materials Design,” *Computational Materials System Design*, D. Shin and J. Saal, eds., Springer, Cham, pp. 1–25.

[9] Horstemeyer, M. F., 2012, *Integrated Computational Materials Engineering (ICME) for Metals: Using Multiscale Modeling to Invigorate Engineering Design With Science*, John Wiley & Sons, Hoboken, NJ.

[10] Shahan, D. W., and Seepersad, C. C., 2012, “Bayesian Network Classifiers for Set-Based Collaborative Design,” *ASME J. Mech. Des.*, 134(7), p. 071001.

[11] Matthews, J., Klatt, T., Morris, C., Seepersad, C. C., Haberman, M., and Shahan, D., 2016, “Hierarchical Design of Negative Stiffness Metamaterials Using a Bayesian Network Classifier,” *ASME J. Mech. Des.*, 138(4), p. 041404.

[12] Li, C., and Mahadevan, S., 2016, “Role of Calibration, Validation, and Relevance in Multi-Level Uncertainty Integration,” *Reliab. Eng. Syst. Saf.*, 148, pp. 32–43.

[13] Mullins, J., and Mahadevan, S., 2016, “Bayesian Uncertainty Integration for Model Calibration, Validation, and Prediction,” *J. Verification, Validation and Uncertainty Quantification*, 1(1), p. 011006.

[14] Kalidindi, S. R., 2015, *Hierarchical Materials Informatics: Novel Analytics for Materials Data*, Elsevier, Waltham, MA.

[15] McDowell, D. L., and Kalidindi, S. R., 2016, “The Materials Innovation Ecosystem: A Key Enabler for the Materials Genome Initiative,” *MRS Bulletin*, 41(4), pp. 326–337.

[16] McDowell, D. L., and LeSar, R. A., 2016, “The Need for Microstructure Informatics in Process–Structure–Property Relations,” *MRS Bulletin*, 41(8), pp. 587–593.

[17] Panchal, J. H., Kalidindi, S. R., and McDowell, D. L., 2013, “Key Computational Modeling Issues in Integrated Computational Materials Engineering,” *Comput. Aided Des.*, 45(1), pp. 4–25.

[18] McDowell, D. L., and Olson, G., 2008, “Concurrent Design of Hierarchical Materials and Structures,” *Sci. Model. Simul.*, 15(1–3), pp. 207–240.

[19] Simon, H. A., 2013, *Administrative Behavior*, Simon and Schuster, New York, NY.

[20] Adams, B. L., Kalidindi, S., and Fullwood, D. T., 2013, *Microstructure-Sensitive Design for Performance Optimization*, Butterworth-Heinemann, Waltham, MA.

[21] Kalidindi, S. R., Niezgod, S. R., Landi, G., Vachhani, S., and Fast, T., 2010, “A Novel Framework for Building Materials Knowledge Systems,” *Computers, Materials & Continua*, 17(2), pp. 103–125.

[22] Kalidindi, S. R., Niezgod, S. R., and Salem, A. A., 2011, “Microstructure Informatics Using Higher-Order Statistics and Efficient Data-Mining Protocols,” *JOM*, 63(4), pp. 34–41.

[23] Choi, H.-J., Austin, R., Allen, J. K., McDowell, D. L., Mistree, F., and Benson, D. J., 2005, “An Approach for Robust Design of Reactive Power Metal Mixtures Based on Non-Deterministic Micro-Scale Shock Simulation,” *J. Computer-Aided Mater. Des.*, 12(1), pp. 57–85.

[24] Choi, H.-J., McDowell, D. L., Allen, J. K., and Mistree, F., 2008, “An Inductive Design Exploration Method for Hierarchical Systems Design Under Uncertainty,” *Eng. Optim.*, 40(4), pp. 287–307.

[25] Nellippallil, A. B., Rangaraj, V., Gautham, B., Singh, A. K., Allen, J. K., and Mistree, F., 2018, “An Inverse, Decision-Based Design Method for Integrated Design Exploration of Materials, Products, and Manufacturing Processes,” *ASME J. Mech. Des.*, 140(11), p. 111403.

[26] Chen, W., Simpson, T. W., Allen, J. K., and Mistree, F., 1999, “Satisfying Ranged Sets of Design Requirements Using Design Capability Indices as Metrics,” *Eng. Optim.*, 31(5), pp. 615–619.

[27] Majta, J., Kuziak, R., Pietrzyk, M., and Krzton, H., 1996, “Use of the Computer Simulation to Predict Mechanical Properties of C-Mn Steel, After Thermomechanical Processing,” *J. Mater. Process. Technol.*, 60(1–4), pp. 581–588.

[28] Kuziak, R., Cheng, Y.-W., Glowacki, M., and Pietrzyk, M., 1997, “Modeling of the Microstructure and Mechanical Properties of Steels During Thermomechanical Processing,” *NIST Technical Note (USA)*, 1393, p. 72.

[29] Gladman, T., McIvor, I., and Pickering, F., 1972, “Some Aspects of the Structure-Property Relationships in High-C Ferrite-Pearlite Steels,” *J. Iron Steel Inst.*, 210(12), pp. 916–930.

[30] Gladman, T., Dulieu, D., and McIvor, I. D., 1977, “Structure/Property Relationships in High-Strength Micro-Alloyed Steels,” *Proceedings of Conference on Microalloying*, ‘75, pp. 32–55.

[31] Yada, H., 1987, “Prediction of Microstructural Changes and Mechanical Properties in Hot Strip Rolling,” *International Symposium on Accelerated Cooling Rolled Steel*, Winnipeg, MB, Canada, Aug. 24–25, pp. 105–119.

[32] Pietrzyk, M., Cser, L., and Lenard, J., 1999, *Mathematical and Physical Simulation of the Properties of Hot Rolled Products*, Elsevier, Kidlington, Oxford.

[33] Phadke, S., Pauskar, P., and Shivpuri, R., 2004, “Computational Modeling of Phase Transformations and Mechanical Properties During the Cooling of Hot Rolled Rod,” *J. Mater. Process. Technol.*, 150(1), pp. 107–115.

- [34] Taguchi, G., and Clausing, D., 1990, "Robust Quality," *Harv. Bus. Rev.*, **68**(1), pp. 65–75.
- [35] Mistree, F., Hughes, O. F., and Bras, B., 1993, "Compromise Decision Support Problem and the Adaptive Linear Programming Algorithm," *Prog. Astronaut. Aeronaut.*, **150**, p. 251.
- [36] Nellippallil, A., De, P., Gupta, A., Goyal, S., and Singh, A., 2016, "Hot Rolling of a Non-Heat Treatable Aluminum Alloy: Thermo-Mechanical and Microstructure Evolution Model," *Trans. Indian Inst. Met.*, pp. 1–12.
- [37] Hodgson, P., and Gibbs, R., 1992, "A Mathematical Model to Predict the Mechanical Properties of Hot Rolled C-Mn and Microalloyed Steels," *ISIJ Int.*, **32**(12), pp. 1329–1338.
- [38] Jägle, E., 2007, "Modelling of Microstructural Banding During Transformations in Steel," Ph.D. dissertation, Department of Materials Science & Metallurgy, University of Cambridge, Cambridge, UK.
- [39] Jones, S., and Bhadeshia, H., 1997, "Kinetics of the Simultaneous Decomposition of Austenite Into Several Transformation Products," *Acta Mater.*, **45**(7), pp. 2911–2920.
- [40] Jones, S., and Bhadeshia, H., 1997, "Competitive Formation of Inter- and Intragranularly Nucleated Ferrite," *Metall. Mater. Trans. A*, **28**(10), pp. 2005–2013.
- [41] Myers, R. H., Montgomery, D. C., and Anderson-Cook, C. M., 2016, *Response Surface Methodology: Process and Product Optimization Using Designed Experiments*, R. H. Meyers, D. C. Montgomery, eds., A Wiley-Interscience Publications, Hoboken, NJ.
- [42] Mistree, F., and Kamal, S., 1985, *DSIDES: Decision Support in the Design of Engineering Systems*, University of Houston, Houston, TX.
- [43] Nellippallil, A. B., Song, K. N., Goh, C.-H., Zagade, P., Gautham, B., Allen, J. K., and Mistree, F., 2017, "A Goal-Oriented, Sequential, Inverse Design Method for the Horizontal Integration of a Multistage Hot Rod Rolling System," *ASME J. Mech. Des.*, **139**(3), p. 031403.